Design and stress analysis of femur bone implant with composite plates

S. Ramakrishna* and B. Pavani[a]

Department of Mechanical Engineering, Gayatri Vidya Parishad College of Engineering (Autonomous), Madhurawada, Visakhapatnam-530048, Andhra Pradesh, India

Abstract. Development of lightweight implant plates are important to reduce the stress shielding effect for a prosthesis of femur bone fractures. Stainless steel (SS-316L) is a widely used material for making implants. Stress shielding effect and other issues arise due to the difference in mechanical properties of stainless steel when compared with bone. To overcome these issues, composite materials seem to be a better alternative solution. The comparison is made between two biocompatible composite materials, namely Ti-hydroxyapatite and Ti-polypropylene. "Titanium (Ti)" is fiber material while "hydroxyapatite" and "polypropylene" are matrix materials. These two composites have Young's modulus closer to the bone than stainless steel. Besides the variety of bones, present paper constrained to femur bone analysis only. Being heaviest and longest, the femur is the most likely to fail among all bone failures in human. Modelling of the femur bone, screws, implant and assembly was carried out using CATIA and static analysis was carried out using ANSYS. The femur bone assembly was analyzed for forces during daily activities. Ti-hydroxyapatite and Ti-polypropylene composite implants induced more stress in composite implant plate, results less stress induced in bone leading to a reduction in shielding effect than stainless steel implant plate thus ensuring safety and quick healing for the patient.

Keywords: fracture fixation plate; implant; composite; stress shielding effect; femur bone

1. Introduction

Femur bone is the largest bone in the human body and connects the knee and the hip joint. Bone is a composite material with matrix hydroxyapatite and collagen fibers. Experimental investigations were carried out to obtain the material properties of human femur bone (Wirtz *et al.* 2000). Mechanical strength characteristics of the femoral neck obtained by finite element method and correlated with bone mineral density (Tsouknidas *et al.* 2012). Stainless steel plates are frequently used in orthopedic surgery for repairing fractures and for fixing ends of the broken bones. As a part of the case study, failure analysis was carried out on the femoral stem with an implant with steel plates and found that fretting and crevice corrosion are cause for the failure of the hip implant (Stronach *et al.* 2016).

Wear and corrosion of steel implants are the main factors for the breakage of steel implants

---

*Corresponding author, Associate Professor, E-mail: sramakrishna@gvpce.ac.in
[a]Student, E-mail: pavanibathina.mech@gmail.com

Table 1 Mechanical properties of fiber and matrix materials (Arifin *et al.* 2014, Wang 2016)

Properties	Fiber	Properties	Matrix	
	Titanium		Hydroxyapatite	Polypropylene
E_f (GPa)	116	E_m(GPa)	13	0.9
G_f (GPa)	43	G_m (GPa)	5.12	0.42
ϑ_f	0.34	ϑ_m	0.27	0.45

(Petkovic *et al.* 2012). After the implant was inserted into the femur the phenomena of stress shielding occurred. The load which is originally transferred to the bone, now it was transferred through the implant. Bone acting as a structure to resist the force acting upon it, based on Wolff's law. This was the main problem occurred during surgery in fixing implants in hip joint, further leads to bone loss (Bergmann *et al.* 1995, Ridzwan *et al.* 2007). Titanium-based biomaterials are useful for preventing stress shielding between bone and implant devices. Low Young's modulus of titanium alloys is expected to be useful in practical applications such as implant devices used for replacing failed hard tissue (Niinomi and Nakai 2011). Composites are currently recognized as the class of materials with the highest performance and have been used in biomedical applications (Florea and Carcea 2012). Polyethylene, polypropylene and hydrogel polyurethane are successfully used for prostheses or body organs replacement (Wang 2016). Combining hydroxyapatite with a higher mechanical strength biocompatible material such as a titanium (Ti) alloy to form a composite. They would possess characteristics essential to modern implant materials, such as bio-inertness, a low Young's modulus, and high biocompatibility (Arifin *et al.* 2014, Sopyana *et al.* 2007). Forces and torques acting on hip joint are computed using free body diagram then finite element analysis carried on hip joint determine the stress distribution and deformations (Madeti *et al.* 2018a, b). Forces acting on femur bone are calculated by using Lami's theorem and finite element analysis is done for a person whose weight varies from 600 N to 1500 N while standing to find stress distribution and deformation on femur bone (Madeti *et al.* 2018a, b). A review on developments in mechanical properties and wear resistance of biomedical Titanium materials processed by High Pressure Torsion (HPT) was presented. HPT is one of the approaches available for improving the mechanical and wear properties of biomedical Titanium materials (Mohammed 2015). A review on experimental studies of knee geometry and forces acting on knee are presented and also discussed static and dynamic analysis of knee joint (Madeti *et al.* 2015). The importance of the mesh quality in the finite element model results was analyzed and presented sensitivity analysis of finite element models for the humeral bone and cartilage structures (Bola *et al.* 2016). Suitable materials for knee implants are compared and performed finite element analysis using ANSYS on knee implant for body weights of 600 N and 1000 N (Madeti *et al.* 2018a, b). Stresses developed in the shoulder muscles during abduction arm movement during the full range of motion was analysed by using the 3D finite element model. 3D scanning (ATOS III scanner) is used for the 3D shoulder joint CAD model generation in CATIA V5 (Metan *et al.* 2016).

2. Elastic properties of the 3D composite plate using MATLAB code

Table 1 shows the material properties of fiber and matrix material obtained from the experimental analysis (Arifin *et al.* 2014, Wang 2016) used for calculation of elastic properties of fiber reinforced

Table 2 Elastic properties of hydroxyapatite lamina

Volume fraction of fiber	V_f=0.4	V_f=0.6	V_f=0.8
E_1 (GPa)	54.2	74.8	95.4
E_2 (GPa)	25.2	36.9	58.97
E_3 (GPa)	25.2	36.9	58.97
G_{12} (GPa)	9.8	14.28	22.53
G_{23} (GPa)	9.3	13.73	22.49
G_{13} (GPa)	9.8	14.28	22.53
ϑ_{12}	0.29	0.31	0.29
ϑ_{23}	0.33	0.34	0.31
ϑ_{13}	0.29	0.31	0.29

composites implant plate. The following theoretical equations (Mallick 2007) are used to development of MATLAB code to find elastic properties of fiber reinforced composites femur bone implant plate at lamina level from individual properties of fiber and matrix. The elastic properties of hydroxyapatite lamina obtained from MATLAB code for different volume fractions are shown in Table 2.

$$E_1 = E_f V_f + E_m(1 - V_f) \tag{1}$$

$$E_2 = E_m \left[\frac{E_f + E_m + (E_f - E_m)V_f}{E_f + E_m - (E_f - E_m)V_f} \right] \tag{2}$$

$$\vartheta_{12} = \vartheta_f V_f + \vartheta_m (1 - V_f) \tag{3}$$

$$V_{23} = \vartheta_f V_f + \vartheta_m (1 - V_f) \left[\frac{1 + \vartheta_m - \vartheta_{12}\left(\frac{E_m}{E_1}\right)}{1 - \vartheta_m^2 + \vartheta_m \vartheta_{12}\left(\frac{E_m}{E_1}\right)} \right] \tag{4}$$

$$G_{12} = G_m \left[\frac{G_f + G_m + (G_f - G_m)V_f}{G_f + G_m - (G_f - G_m)V_f} \right] \tag{5}$$

$$G_{23} = \frac{E_2}{2(1 + \vartheta_{23})} \tag{6}$$

Majority of experiment results show that $E_2 = E_3$, $G_{12} = G_{31}$, $\vartheta_{12} = \vartheta_{31}$ where E_1=Young's modulus in the longitudinal direction, E_2=Young's modulus in the transverse direction, E_f=Young's modulus of fiber, E_m=Young's modulus of matrix, ϑ_f= Poisson ratio of fiber, ϑ_m=Poisson ratio of matrix, G_f=Shear modulus of fiber, G_m=Shear modulus of matrix, G_{12}=In-plane shear modulus, ϑ_{12}=Poisson ratio.

Composite properties are dependent on volume fractions of fiber and matrix and orientation of individual lamina. Properties of lamina are calculated by using volume fraction and individual

Table 3 Elastic properties of hydroxyapatite laminate

| Ply orientation	E_x (GPa)	E_y (GPa)	E_z (GPa)	G_{xy} (GPa)	G_{yz} (GPa)	G_{xz} (GPa)	ϑ_{xy}	ϑ_{yz}	ϑ_{zx}
[0, 90, 45, 0, 90,45, 0, 90]	37.15	37.15	25.72	11.42	9.54	9.549	0.23	0.30	0.30
[0, 90, 0, 90, 0, 90, 0, 90]	39.91	39.92	25.76	9.80	9.55	9.55	0.18	0.32	0.32
[90, 45, 90, 45, 90, 45, 90,45]	26.88	40.79	25.42	12.72	9.67	9.42	0.22	0.26	0.29
[0, 45, 0, 45, 0, 45, 0, 45]	40.79	26.88	25.42	12.72	9.897	9.897	0.34	0.29	0.26
[0, 0, 0, 0, 0, 0, 0, 0]	58.20	25.20	25.20	9.80	9.30	9.80	0.29	0.33	0.29
[90, 90, 90, 90, 90, 90, 90, 90]	25.20	54.20	25.20	9.80	9.20	9.30	0.13	0.29	0.33
[45, 45, 45, 45, 45, 45, 45, 45]	26.76	26.76	25.2	14.52	9.54	9.54	0.36	0.24	0.24
[30, 90, 30, 90, 30, 90, 30, 90]	30.87	39.42	25.57	11.78	9.611	9.48	0.22	0.28	0.29
[90, 60, 90, 60, 90, 60, 90, 60]	25.20	44.75	25.30	11.96	9.736	9.36	0.19	0.26	0.30
[30, 60, 30, 60, 30, 60, 30, 60]	30.14	30.14	25.30	13.34	9.54	9.54	0.30	0.27	0.27
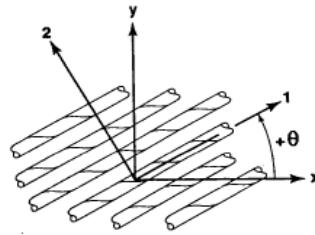
Fig. 1 Directions of fiber and the principal axis
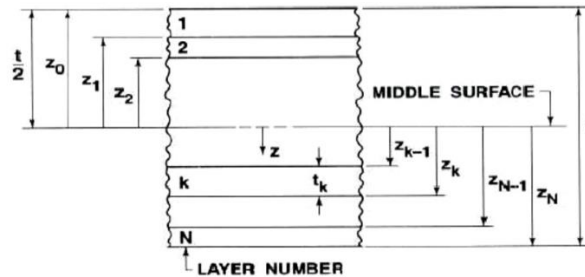
Fig. 2 Geometry of an N-layered laminate

elastic properties of fiber and matrix. Laminate properties depend up on orientation of individual lamina and these properties can be found by using A, B and D matrices (Mallick 2007). The properties lamina shown in Table 2 are used to calculate the 3-dimensional properties of laminate. The following micro-macro mechanics equations (Mallick 2007) based on laminate theory are used to develop MATLAB code for elastic properties of laminate using the individual properties of fiber, matrix and lay-up sequence. Table 3 represents the elastic properties of hydroxyapatite laminate obtained from MATLAB code for different ply orientations. These material properties are used for optimisation of ply orientation in the next section 3. Figs. 1 and 2 indicate material directions with respect to the principle axis and geometry of laminate (Mallick 2007).

Stress-strain relations for a lamina of arbitrary orientation are

$$\begin{bmatrix} \sigma_x \\ \sigma_y \\ \tau_{xy} \end{bmatrix} = [q] \begin{bmatrix} \varepsilon_x \\ \varepsilon_y \\ \gamma_{xy} \end{bmatrix} = \begin{bmatrix} q_{11} & q_{12} & q_{16} \\ q_{21} & q_{22} & q_{26} \\ q_{16} & q_{26} & q_{66} \end{bmatrix} \begin{bmatrix} \varepsilon_x \\ \varepsilon_y \\ \gamma_{xy} \end{bmatrix} \tag{7}$$

Q_{ij} is reduced stiffness matrix and

$$Q_{11} = \frac{E_1}{1 - \vartheta_{12}\vartheta_{21}}, Q_{22} = \frac{E_2}{1 - \vartheta_{12}\vartheta_{21}}, Q_{12} = \frac{\vartheta_{21}E_1}{1 - \vartheta_{12}\vartheta_{21}}, Q_{66} = G_{12} \tag{8}$$

q_{ij} is transformed reduced stiffness matrix, where

$$\begin{aligned} q_{11} &= Q_{11}\cos^4\theta + Q_{22}\sin^4\theta + (2Q_{12} + 4Q_{66})\cos^2\theta\sin^2\theta \\ q_{22} &= Q_{11}\sin^4\theta + Q_{22}\cos^4\theta + (2Q_{12} + 4Q_{66})\cos^2\theta\sin^2\theta \\ q_{12} &= (Q_{11} + Q_{22} - 4Q_{66})\cos^2\theta\sin^2\theta + Q_{12}(\cos^4\theta + \sin^4\theta) \\ q_{16} &= (Q_{11} - Q_{12} - 2Q_{66})\cos^3\theta\sin\theta + (Q_{12} - Q_{22} + 2Q_{66})\cos^3\theta\sin\theta \\ q_{26} &= (Q_{11} - Q_{12} - 2Q_{66})\sin^3\theta\cos\theta + (Q_{12} - Q_{22} + 2Q_{66})\sin^3\theta\cos\theta \\ q_{66} &= (Q_{11} + Q_{22} - 2Q_{12} - 2Q_{66})\cos^2\theta\sin^2\theta + Q_{66}(\cos^4\theta + \sin^4\theta) \end{aligned} \tag{9}$$

Stress-Strain variation in laminate is

$$\begin{bmatrix} N_x \\ N_y \\ N_{xy} \end{bmatrix} = \begin{bmatrix} A_{11} & A_{12} & A_{16} \\ A_{21} & A_{22} & A_{26} \\ A_{16} & A_{26} & A_{66} \end{bmatrix} \begin{bmatrix} \varepsilon_x{}^0 \\ \varepsilon_y{}^0 \\ \gamma_{xy}{}^0 \end{bmatrix} + \begin{bmatrix} B_{11} & B_{12} & B_{16} \\ B_{21} & B_{22} & B_{26} \\ B_{16} & B_{26} & B_{66} \end{bmatrix} \begin{bmatrix} k_x \\ k_y \\ k_{xy} \end{bmatrix} \tag{10}$$

$$\begin{bmatrix} M_x \\ M_y \\ M_{xy} \end{bmatrix} = \begin{bmatrix} B_{11} & B_{12} & B_{16} \\ B_{21} & B_{22} & B_{26} \\ B_{16} & B_{26} & B_{66} \end{bmatrix} \begin{bmatrix} \varepsilon_x{}^0 \\ \varepsilon_y{}^0 \\ \gamma_{xy}{}^0 \end{bmatrix} + \begin{bmatrix} D_{11} & D_{12} & D_{16} \\ D_{21} & D_{22} & D_{26} \\ D_{16} & D_{26} & D_{66} \end{bmatrix} \begin{bmatrix} k_x \\ k_y \\ k_{xy} \end{bmatrix} \tag{11}$$

where

$$A_{ij} = \sum_{k=1}^{N} (q_{ij})_k (Z_k - Z_{k-1}) \tag{12}$$

$$B_{ij} = \frac{1}{2}\sum_{k=1}^{N} (q_{ij})_k (Z_k{}^2 - Z_{k-1}{}^2) \tag{13}$$

$$D_{ij} = \frac{1}{3}\sum_{k=1}^{N} (q_{ij})_k (Z_k{}^3 - Z_{k-1}{}^3) \tag{14}$$

3. Optimization of ply sequence of composite plate

Static analysis of femur bone fracture fixation composite plate (implant plate) is carried out using ANSYS APDL for optimization of ply sequence for minimization of von Mises stress. For this purpose, randomly selected ply orientations of 8 layers are considered in the present

Table 4 Stress in different ply orientations

Ply orientation	von Mises stress (MPa) in top layer
[0, 90, 45, 0, 90, 45, 0, 90]	194.24
[0, 90, 0, 90, 0, 90, 0, 90]	185.30
[90, 45, 90, 45, 90, 45, 90, 45]	207.12
[0, 45, 0, 45, 0, 45, 0, 45]	207.04
[0, 0, 0, 0, 0, 0, 0, 0]	180.05
[90, 90, 90, 90, 90, 90, 90, 90]	184.15
[45, 45, 45, 45, 45, 45, 45, 45]	184.92
[30, 90, 30, 90, 30, 90, 30, 90]	197.04
[90, 60, 90, 60, 90, 60, 90, 60]	193.68
[30, 60, 30, 60, 30, 60, 30, 60]	189.70
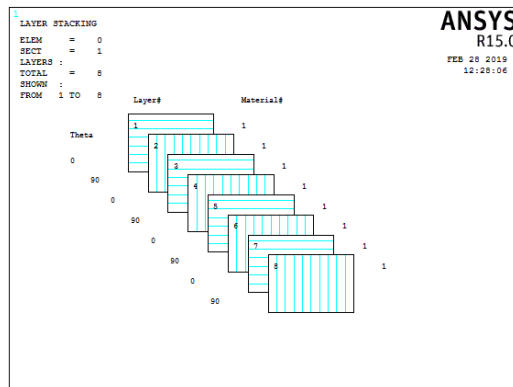
Fig. 3 Ply orientation in composite plate [0, 90, 0, 90, 0, 90, 0, 90]

optimization study as shown in Table 4. Femur bone composite implant plate is designed with a length of 100 mm, the width of 25 mm and thickness of 2 mm in CATIA and the model was exported into ANSYS APDL for carrying out static analysis. Bottom of the plate is fixed and pressure load is applied on the top of the plate. 4-nodded shell 181 elements are used to generate the grid for a composite plate. The thickness of each layer is considered as 0.25 mm, so a total of 8 layers are used to generate the femur bone composite plate thickness of 2 mm. Table 4 represents static analysis results in ANSYS APDL with different ply orientations. Fig. 3 represents the sample ply orientation in composite plate [0, 90, 0, 90, 0, 90, 0, 90] used for analysis using ANSYS APDL. Form the optimization study it is observed that laminate with lay-up sequence of [0, 0, 0, 0, 0, 0, 0, 0, 0] has least von Mises stress (180.05 MPa) compared to all other ply orientations as shown in Fig. 4. The optimised ply orientation [0, 0, 0, 0, 0, 0, 0, 0, 0] is used for analysis of cracked femur bone with composite fracture fixation plate in the next section 4.

4. Modelling and analysis of femur bone implant with composite plate

Femur bone model was generated using CATIAV5 as per geometrical data taken in the form of CT scan image of 17 years old male of weight 75 kg (Shireesha *et al*. 2013) and bone material
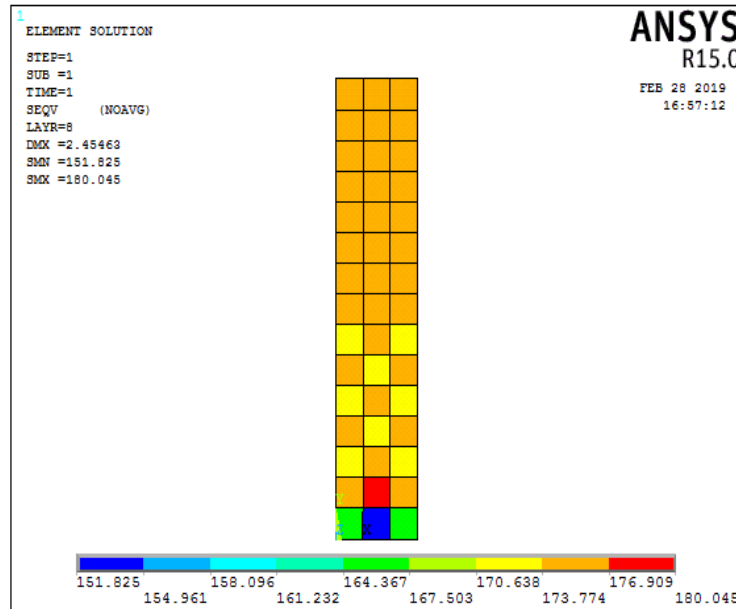
Fig. 4 von Mises stress in optimized laminate [0, 0, 0, 0, 0, 0, 0, 0]


| (a) Without crack | (b) With crack |
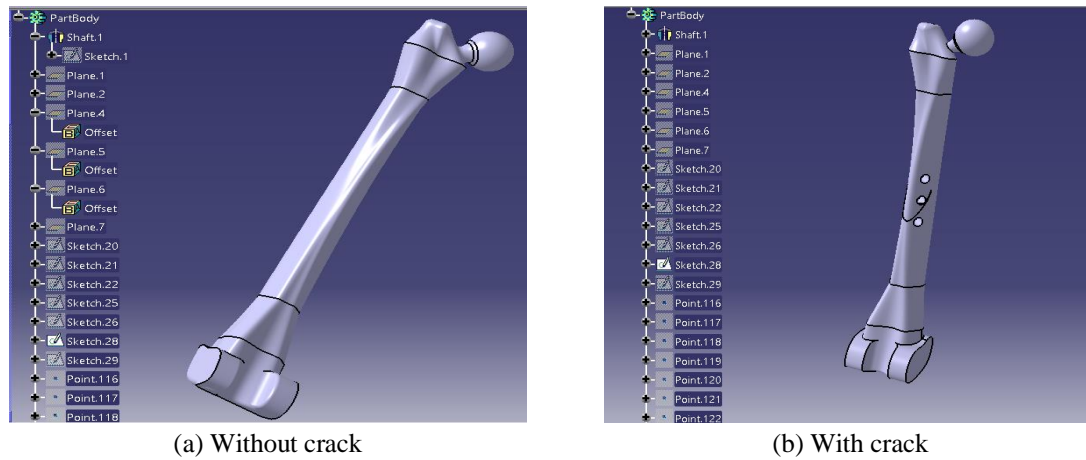
Fig. 5 Solid model of femur bone

properties obtained from experimental investigations (Wirtz *et al.* 2000) are used in the present analysis. Femoral head femur bone was generated with neck shaft angle of 122.9° with diameter of 43.4 mm. The length and width of femur bone was taken as 443.6 mm and 75.6 mm respectively. Fig. 5 represents a solid model of femur bone with and without crack. The implant plates are designed with 3-holes and 4-holes for comparison of induced von Mises stress and to find the best design for the composite plate as an implant for femur bone. Solid models of femur bone implant plate with 3-holes and 4-holes are shown in Fig. 6. The material properties of the optimized laminate obtained in section 3 are applied to femur bone implant plates for the simulation of von Mises stress using ANSYS.

Assembly of the cracked femur bone and implant plate with screws have been designed using
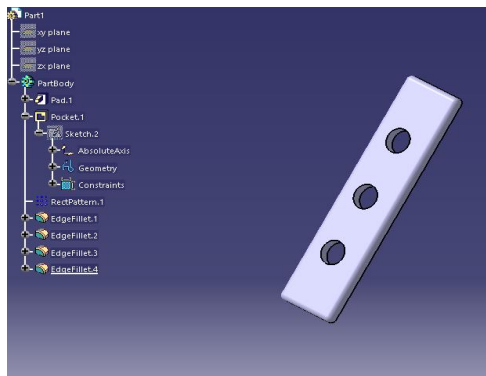
(a) 3-hole implant plate
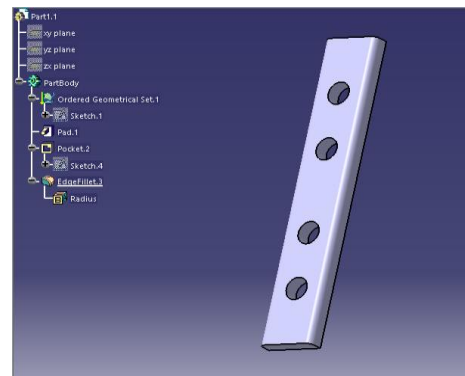
(b) 4-hole implant plate

Fig. 6 Solid model of femur bone implant plate
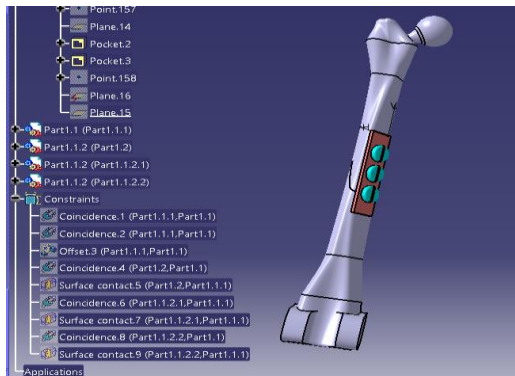
(a) 3-hole implant plate
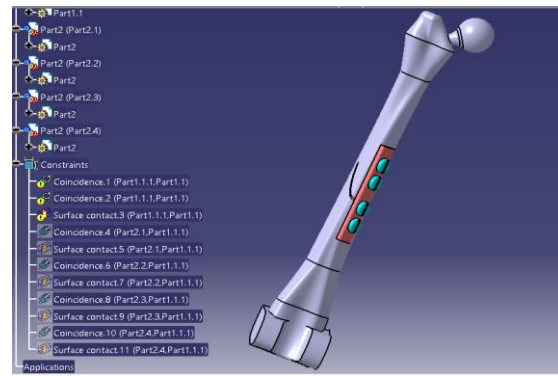
(b) 4-hole implant plate

Fig. 7 Solid model of femur bone 3-hole implant plate
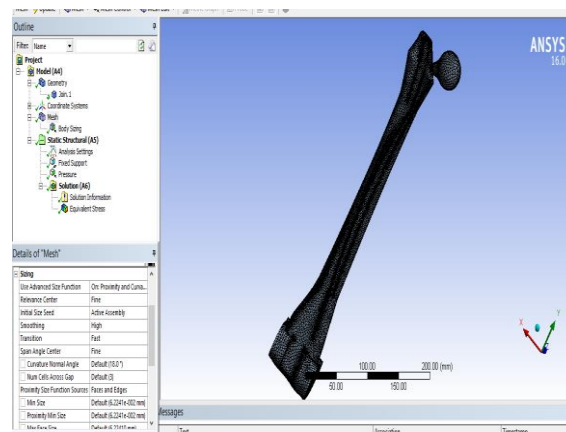
Fig. 8 Meshed model of femur bone

CATIA. Solid models of femur bone with 3-hole and 4-hole implant plates are shown in Fig. 7. The solid models generated in CATIA are imported into ANSYS in IGES format. Four-node shell
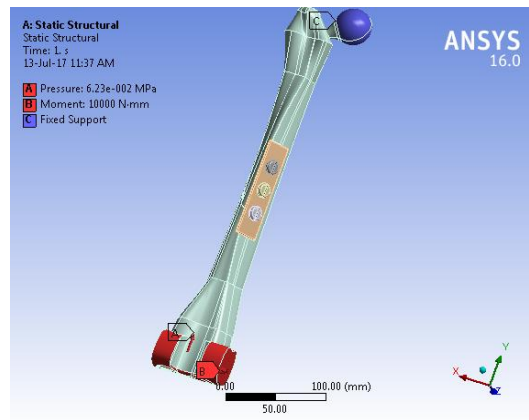
Fig. 9 The boundary condition of femur bone

Table 6 Results of the 3-hole design of femur bone with the composite implant plate

	von Mises Stress (MPa)		
	Stainless steel implant plate	Composite implant plate	
Condition	SS-316	Ti-hydroxyapatite	Ti-polypropylene
Running	9.78	12.87	18.25
Jumping	5.42	7.97	11.28
Walking	4.76	7.33	10.05
Standing	3.23	6.11	8.85

181 elements are used for meshing the present model. Grid convergence study is very important to ensure the results are independent of the number of elements in the final meshed model. For this purpose, a graph is plotted between element size and von Mises stress. The element seizes are varied from 12 mm to 1 mm. As element size decreases, stress becomes almost constant from element size 3 mm. So, this element size 3 mm is considered in the present analysis. After convergence the number of nodes and elements generated final meshed model are 71553 and 40502 respectively. The dynamic loads of 735 N, 785 N, 850 N and 1410 N are applied on the femur bone in daily activities of standing, walking, jumping and running respectively. Also considered the maximum moment of 10,000 N-mm applied to compensate the eccentricity of the load in all daily activities. Load and moment are applied on the knee joint and fixed support is applied in the femoral head. The meshed model and boundary conditions of femur bone with a composite implant plate are shown in Figs. 8 and 9 respectively.

5. Results and discussion

Table 6 indicates the von Mises stress induced in femur bone composite implant plate obtained from ANSYS. From these results, it is observed that the stresses induced in the composite implant plate are higher when compared with stainless steel implant plate. This is due to maximum load is transferred to composite implant plate when compared with steel plate. The load transferred to the
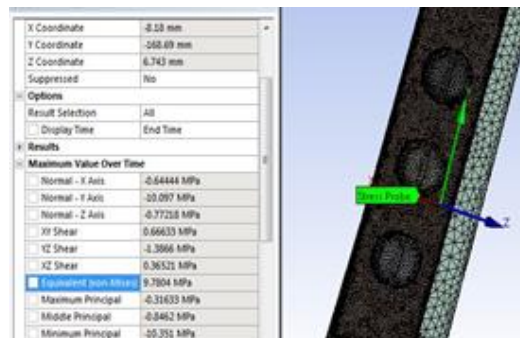
Fig. 10 Stress contour of stainless steel plate
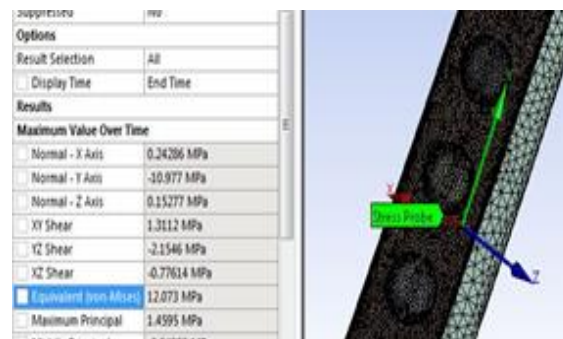
Fig. 11 Stress contour of Ti-hydroxyapatite composite implant plate
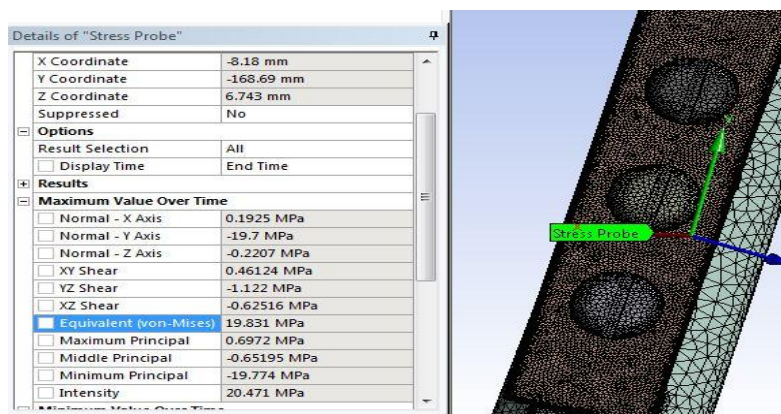
Fig. 12 Stress contour of Ti-Polypropylene composite implant plate

femur bone is less in composite implant plate when compared with stainless steel implant plate. Thus, the composite implant plates are best suitable to overcome the stress shielding effect in femur bone and ensuring quick healing for the patient. The present paper focuses on the design of composite implant plate, so stress comparison is presented in that plate only. Fig. 10 clearly shows the von Mises stress results for the 3-hole design of stainless steel implant plate. All results are presented and compared at maximum stressed element located near the middle hole of all 3-hole and 4-hole composite implant plate designs. Figs. 11 and 12 indicate the distribution of von Mises
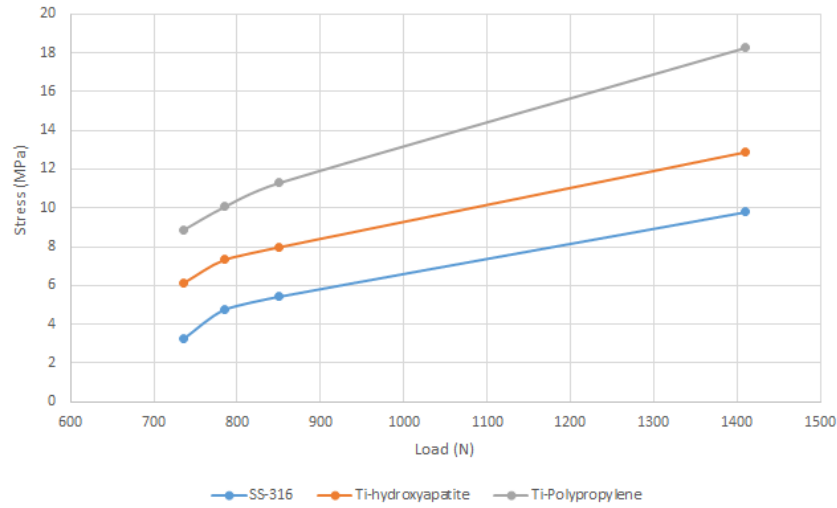
Fig. 13 Variation of stress with respect to load for 3-hole design implant plates

Table 7 Results of the 4-hole design of femur bone with the composite implant plate

	von Mises Stress (MPa)		
	Stainless steel plate	Composite implant plate	
Condition	SS-316	Condition	SS-316
Running	11.48	Running	11.48
Jumping	7.19	Jumping	7.19
Walking	6.44	Walking	6.44
Standing	5.51	Standing	5.51

stress induced in 4-hole design of Ti-hydroxyapatite and Ti-Polypropylene composite implant plates respectively.

From the static analysis, it observed that percentage increment of stress in Ti-hydroxyapatite composite implant plate with the 3-hole design when compared with stainless steel implant plate is 31.5% and for Ti-polypropylene composite implant plate with the 3-hole design is 86.6% in running activity. Percentage increment of stress in Ti-polypropylene composite implant plate, when compared with Ti-hydroxyapatite composite plate is 41.8% in running activity. The variation of maximum stress with respect to load is shown in Fig. 13. The stress ranged from 3.2 MPa to 9.78 MPa for stainless steel implant plate, 6.11 MPa to 12.87 MPa for Ti-hydroxyapatite composite implant plate and 8.85 MPa to 18.25 MPa for Ti-Polypropylene composite implant plate in daily activities of running, jumping, walking and standing in 3-hole design implant plate.

Table 7 shows the von Mises stresses in the 4-hole design of composite implant plate. Stress analysis on the 4-hole design of femur bone implant indicates the percentage increment of stress in Ti-hydroxyapatite composite plate when compared with the stainless plate is 27.1% in running activity. Similarly, percentage increment of stress in Ti-polypropylene compared with a stainless plate is 72.7% in running activity. Percentage increment of stress in Ti-polypropylene compared with Ti-hydroxyapatite is 35.9% in running activity. The variation of maximum stress with respect to load for 4-hole design implant is shown in Fig. 14. The stress for ranged from 5.51 MPa to 11.48
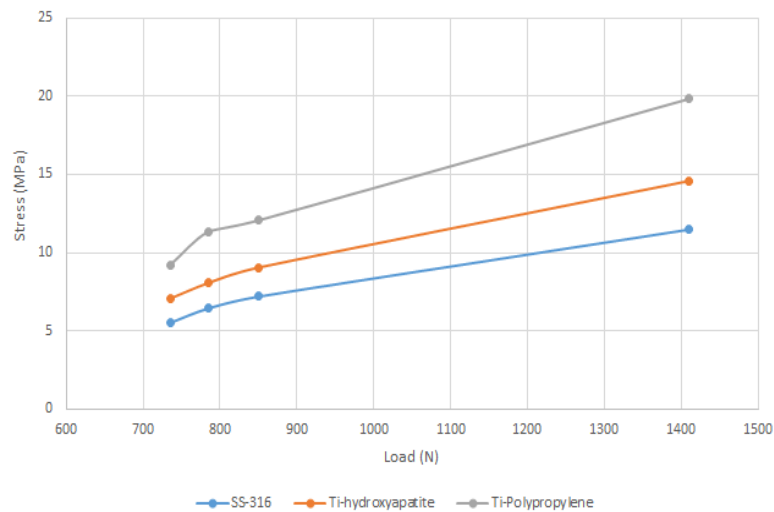
Fig. 14 Variation of stress with respect to load for 4-hole design implant plates

MPa for steel implant plate, 7.07 MPa to 14.59 MPa for Ti-hydroxyapatite composite implant plate and 9.21 MPa to 19.78 MPa for Ti-Polypropylene composite implant in daily activities of running, jumping, walking and standing in 4-hole design implant plate. More stresses are developed in 4-hole design of femur bone implant when compared with 3-hole design of femur bone implant for same loading conditions. It indicates that 4-hole design of femur bone composite implant plate is best suitable for present application to reduce the stress shielding effect in femur bone because it transfers less load to the bone compared to 3-hole design of femur bone composite implant plate.

5. Conclusions

Modelling and static analysis of femur bone implant with two different composite plates are carried out by using CATIA and ANSYS respectively. To overcome the stress shielding effect, the stainless steel implant material is replaced with composite plates, which are having the nearest Young's modulus with the bone than stainless steel. Elastic properties of two composites materials (Ti-hydroxyapatite and Ti-Polypropylene) are calculated at lamina and laminate with different ply orientation using MATLAB code. Then optimisation study is carried out on randomly selected ply orientations of 8 layers. The optimised ply orientation from the optimisation study is used for static analysis of femur bone composite implant plates with Ti-hydroxyapatite and Ti-Polypropylene. The femur bone assembly is analysed for hip contact forces during daily activities of running, jumping, walking and standing. From the static analysis on femur bone implant with composite plates, it is found that more stresses are induced in Ti-hydroxyapatite and Ti-Polypropylene composite plate, because maximum load is transferred to the composite plate when compared to steel plate for the same loading conditions. It indicates that less load is transferred to femur bone with Ti-hydroxyapatite and Ti-Polypropylene composite implant plate than steel implant plate. From these results, it is concluded that composite implant plates are better materials than steel implant plates to overcome the stress shielding effect in femur bone. Form the review of literature it is concluded that the degrading time of composite implant is more than 24 months (Xu *et al*. 2018). When compared

with two composites implant plates, 4-hole design of femur bone implant plate with Ti-polypropylene is the best material followed by Ti-hydroxyapatite to overcome the stress shielding effect of the femur bone. Therefore, safety and quick healing ensured for the patient with 4-hole design of Ti-polypropylene composite implant plate for femur bone.

References

Arifin, A., Sulong, A.B., Muhamad, N., Syarif, J. and Ramli, M.I. (2014), "Material processing of hydroxyapatite and titanium alloy (HA/Ti) composite as implant materials using powder metallurgy", *Mater. Des.*, **55**, 165-175. https://doi.org/10.1016/j.matdes.2013.09.045.

Bergmann, G., Graichen, F. and Rohlmann, A. (1995), "Is staircase walking a risk for the fixation of hip implants", *J. Biomech.*, **28**(5), 535-553. https://doi.org/10.1016/0021-9290(94)00105-D.

Bola, A.M., Ramos, A. and Simões, J.A. (2016), "Sensitivity analysis for finite element modeling of humeral bone and cartilage", *Biomater. Biomech. Bioeng.*, **3**(2), 71-84. https://doi.org/10.12989/bme.2016.3.2.071.

Florea, R.M. and Carcea, I. (2012), "Polymer matrix composites – routes and properties", *Int. J. Mod. Manuf. Technol.*, **4**(1), 59-64.

Madeti, B.K., Chalamalasetti, S.R. and Bollapragada, S.S.S.R. (2015), "Biomechanics of knee joint: Review", *Front. Mech. Eng.*, **10**(2), 176-186. https://doi.org/10.1007/s11465-014-0306-x.

Madeti, B.K., Chalamalasetti, S.R. and Priya Gugulothu, S. (2018a), "Buckling and failure analysis of bonesin hip joint", *J. Mech. Med. Biol.*, **18**(5), 1850052. https://doi.org/10.1142/S0219519418500525.

Madeti, B.K., Chalamalasetti, S.R. and Bollapragada, S.S.S.R. (2018b), "Force evaluation and stress distribution at possible weight and structure of femur bone in pelvis frame while standing", *Int. J. Med. Eng. Inform.*, **10**(3), 235-251. https://doi.org/10.1504/IJMEI.2018.093353.

Mallick, P.K. (2007), *Fiber-Reinforced Composites: Materials, Manufacturing and Design*, CRC Press, New York, U.S.A.

Metan, S.S., Mohankumar, G.C. and Krishna, P. (2016), "Sensitivity analysis of shoulder joint muscles by using the FEM model", *Biomater. Biomech. Bioeng.*, **3**(2), 115-127. https://doi.org/10.12989/bme.2016.3.2.115.

Mohammed, M.T. (2015), "Mechanical and wear properties of HPT-biomedical titanium: A review", *Biomater. Biomech. Bioeng.*, **2**(3), 185-196. http://dx.doi.org/10.12989/bme.2015.2.3.185.

Niinomi, M. and Nakai, M. (2011), "Titanium-based biomaterials for preventing stress shielding between implant devices and bone", *Int. J. Biomater.*, **15**, 836587. https://doi.org/10.1155/2011/836587.

Petkovic, D., Radenkovic, G. and Mitkovic, M. (2012), "Fractographic investigation of failure in stainless steel orthopedic plates", *Facta Univ. Ser. Mech. Eng.*, **10**(1), 7-14.

Ridzwan, M.I.Z., Shuib, S., Hassan, A.Y., Shokri, A.A. and Ibrahim, M.M. (2007), "Problem of stress shielding and improvement to the hip implant designs", *J. Med. Sci.*, **7**(3), 460-467.

Shireesha, Y., Ramana, S.V. and Rao, P.G. (2013), "Modelling and static analysis of femur bone by using different implant materials", *IOSR J. Mech. Civ. Eng.*, **7**(4), 82-91.

Sopyana, I., Melb, M., Rameshc, S. and Khalidd, K.A. (2007), "Porous hydroxyapatite for artificial bone applications", *Sci. Technol. Adv. Mater.*, **8**(1-2), 116-123. https://doi.org/10.1016/j.stam.2006.11.017.

Stronach, B.M., Roach, M.D. and John, K.R.S. (2016), "Failure of Emperion modular femoral stem with implant analysis", *Arthroplast. Today*, **2**(1), 11-14. https://doi.org/10.1016/j.artd.2015.11.004.

Tsouknidas, A., Anagnostidis, K., Maliaris, G. and Michailidis, N. (2012), "Fracture risk in the femoral hip region: A finite element analysis supported experimental approach", *J. Biomech.*, **45**(11), 1959-1964. https://doi.org/10.1016/j.jbiomech.2012.05.011.

Wang, M. (2016), "Optimization of femoral prosthesis based on comprehensive evaluation of structure and material properties", *J. Mech. Med. Biol.*, **16**(8), 5-17. https://doi.org/10.1142/S0219519416400133.

Wirtz, D.C., Schiffers, N., Pandorf, T. and Radermacher, K. (2000), "Critical evaluation of known bone material properties to realize anisotropic FE-simulation of the proximal femur", *Biomechanics*, **31**(10),

1325-1330. https://doi.org/10.1016/S0021-9290(00)00069-5.

Xu, Y., Meng, H., Yin, H., Sun, Z., Peng, J., Xu, X., Guo, Q., Xu, W., Yu, X., Yuan, Z., Xiao, B., Wang, C., Wang, Y., Liu, S., Lu, S., Wang, Z. and Wang, A. (2018), "Quantifying the degradation of degradable implants and bone formation in the femoral condyle using micro-CT 3D reconstruction", *Exp. Ther. Med.*, **15**(1), 93-102. https://doi.org/10.3892/etm.2017.5389.

CC